Structure Characterization of Polyurethanes Containing Poly(dimethylsiloxane)

Mitsuhiro Shibayama,* Masakatsu Suetsugu, Shinichi Sakurai, Tomoyuki Yamamoto, and Shunji Nomura

Department of Polymer Science and Engineering, Kyoto Institute of Technology, Matsugasaki, Sakyo-ku, Kyoto 606, Japan

Received March 13, 1991; Revised Manuscript Received June 18, 1991

ABSTRACT: The degrees of completion in microphase separation for segmented polyurethanes containing a block segment of poly(ethylene oxide)-*b*-poly(dimethylsiloxane)-*b*-poly(ethylene oxide) (PES) were investigated by mechanical and thermal analyses, Fourier transform infrared absorption spectroscopy (FTIR), and small-angle X-ray scattering (SAXS) techniques. These results were compared with those for PES-free polyurethanes having the same molecular weight of the soft segment, M_{PTMG}, where PTMG is the abbreviation of poly(tetramethylene glycol). The 13 wt % of PES addition lowers the capability of crystallization of the major component of the soft segment, PTMG, and increases the degree of completion in microphase separation. A selective surface enrichment was observed for a blend film of polyurethanes with and without PES by FTIR-attenuated total reflection spectroscopy (ATR). The range of enrichment was on the order of a micron, which is much larger than individual molecular size. SAXS analyses showed that these polyurethanes form a microphase-separated structure. The microdomain structure is well described with the hard-segment domains of 60–70 Å long embedded in the soft-segment matrix. The soft-segment chains obey the random-walk statistics in a confined space, which leads to the relation $d_S \sim Z_S^{2/3}$, where d_S and Z_S are the domain size and number-average degree of polymerization of the soft-segment chain.

I. Introduction

According to the recent advancement of medical technology, it is desired to develop polymer materials for medical purposes having a wide variety of functions.[1] Since most of these materials are used in vivo, antithrombogenicity is one of the most important factors to be taken into account as well as suitable mechanical properties. Segmented polyurethane and segmented poly(urethaneurea) are widely used materials for these purposes, particularly for an artificial heart and blood vessel, where elastic properties similar to those of muscle are required as well as antithrombogenicity.[2,3] Mechanical and thermal properties of these polyurethanes and poly(urethaneureas) have been extensively studied in conjunction with their structures by means of a variety of techniques, such as electron microscopy, small- and wide-angle X-ray diffraction (and/or scattering), and Fourier transform infrared spectroscopy and dichroism.[4-20]

Polyurethane containing poly(dimethylsiloxane) in the main chain (coded as KP-13), developed by Kira et al., is one of the most suitable materials for an artificial blood vessel.[21] This is a derivative of a conventional polyurethane (hereafter designated as KP-0) composed of soft (PTMG) and hard (MDI-EG) segments, where PTMG, MDI, and EG denote poly(tetramethylene glycol), 4,4′-diphenylmethane diisocyanate, and ethylene glycol, respectively. In the case of KP-13, some amounts of PTMG chains were substituted by a block segment of poly(ethylene oxide)-*b*-poly(dimethylsiloxane)-*b*-poly(ethylene oxide) (abbreviated to PES). The weight fraction of PES was kept to be 13 wt % so as to optimize the antithrombogenicity without degrading mechanical properties.[21]

We have reported the structure and the orientational behaviors of the KP-13 series (KP-13-650, KP-13-1000, KP-13-2000) by comparing it with a reference polyurethane, KP-0-3000.[22] The sample code is defined to be KP-*x*-*y*, where *x* and *y* are the weight percentage of the PES component and number-average molecular weight of PTMG, M_{PTMG}. It was found that the presence of poly(dimethylsiloxane) (PDMS) components reduced the crystallization capability of the soft segments. These polymers showed no negative orientation of the hard segment although most of the polyurethanes and poly(urethaneureas) did.[6,7,9,12,18,19] This phenomenon was explained with a relatively low cohesive power of the hard-segment domains for KP's. However, due to the lack of a systematic variation of the samples with respect to M_{PTMG}, we could not separate the two contributions, i.e., the effect of PDMS and M_{PTMG}, on the mechanical and thermal properties and morphology.

Two kinds of microphase separation involved in the partial replacement in the soft-segment chains from PTMG to PES have to be considered. One is the microphase separation between hard and soft segments. In the case when the segregation between the hard and soft segments increases with PES addition, the degree of completion in the microphase separation consequently increases. The other is that between PES and PTMG in the soft-segment chains. This may occur due to the strong segregation between PDMS in PES and PTMG. The soft-segment chain, however, should actually be taken as a multiblock copolymer consisting of PES and PTMG. One can see by calculating the stability limit for the microphase transition[23,24] that the microphase-dissolved state becomes stabilized with an increase of the number of blocks for a given composition and total molecular weight of a copolymer. Due to this thermodynamic effect as well as a kinetic effect, the lowering of the degree of completion in the microphase separation between PES and PTMG can also be expected. Therefore, the effects of PES addition into a polyurethane system have to be carefully treated from viewpoints of thermodynamics and/or kinetics of multicomponent polymer systems besides the importance of their technological applications.

In this paper, we examine the two sets of polyurethanes, i.e., KP-0-*y* and KP-13-*y* (*y* = 1000, 2000, and 3000) by viscoelastic measurement, differential scanning calorimetry (DSC), Fourier transform infrared absorption spectroscopy (FTIR), and small-angle X-ray scattering (SAXS).

* To whom correspondence should be addressed.

0024-9297/91/2224-6254$02.50/0

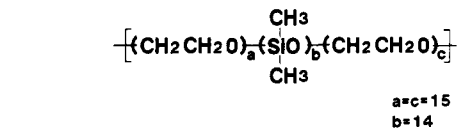

Figure 1. Chemical structure of PES.

Table I
Chemical Composition of the KP Series

code	soft-segment mol wt PTMG	soft-segment mol wt PES	mole fraction MDI/PTMG/PES/EG
KP-0-1000	1025		2/1.15/0/0.85
KP-0-2000	2000		2/0.62/0/1.38
KP-0-3000	2950		2/0.44/0/1.56
KP-13-1000	1025	2400	2/0.94/0.09/0.97
KP-13-2000	2000	2400	2/0.50/0.10/1.40
KP-13-3000	2950	2400	2/0.35/0.10/1.55

First of all, we make a quantitative comparison of the mechanical and thermal properties and of some aspects of the structure, by focusing on the degree of completion in microphase separation and the capability of crystallization of PTMG (sections III.1–III.4). Second, we discuss the degree of completion in microphase separation on stretching a film by FTIR (section III.4). Finally we characterize the domain sizes of the soft and hard segments as a function of the soft-segment molecular weight and discuss the scaling relationship between the domain size and the soft-segment molecular weight (section IV). This result suggests the origin of a lower degree of completion in microphase separation of polyurethanes compared with diblock or triblock copolymers.

II. Experimental Section

Samples. Two series of segmented polyurethanes, KP-13's and KP-0's, were supplied by Kanegafuchi Chemical Industry Co., Ltd. In the case of KP-0's, a prepolymer consisting of PTMG and MDI was first prepared, which was followed by a chain extension reaction with EG. KP-13 series were obtained in a similar manner. However, some fraction of PTMG was substituted by PES. The content of the PES component was 13 wt %. PES is composed of poly(ethylene oxide) (PEO) and PDMS as shown in Figure 1. a–c are the average degrees of polymerization of PEO, PDMS, and PEO, as indicated in the figure. These are determined by titration of the end functional groups and by ^{1}H NMR to be 15, 14, and 15.[25] Table I shows the details of the chemical compositions of the soft and hard segments of KP-13 and KP-0 series. In both series the weight fraction of MDI + EG was kept at 32% so as to keep the hard to soft segment ratio constant. Therefore, the mole fractions of PTMG and EG were systematically varied so as to keep the ratio of MDI to the total. The PTMG's used in this work were purchased from Du Pont Co. The values of M_{PTMG} are listed in the catalog,[25] which were determined by titration of the end hydroxy groups with acetic anhydride. The polydispersity indices were evaluated with gel permeation chromatography (GPC) measurements and were 2.13, 2.00, and 1.89, respectively, for PTMG's having M_{PTMG} = 1025, 2000, and 2950. The details of the sample preparation are described elsewhere.[21]

Films of the KP-13 and KP-0 series were obtained by casting a solution onto a glass plate, dried gradually in an atmosphere of the solvent vapor, a 3:7 mixture of N,N'-dimethylacetamide and 1,4-dioxane. The dried films were peeled off with water, further dried in a vacuum oven kept at 60 °C for 3 days, and then stored in a desiccator until used.

Mechanical and Thermal Properties. Stress–strain and dynamic viscoelastic behaviors were examined with an Autograph IM-100, Shimadzu Corp., and a Rheospectoler DVE-V4, Rheology Co., Ltd., respectively. The details of the experiments were described in the previous paper.[22]

Differential scanning calorimetry (DSC) was conducted with DSC 3100, MAC Science Co., Ltd. The temperature range was

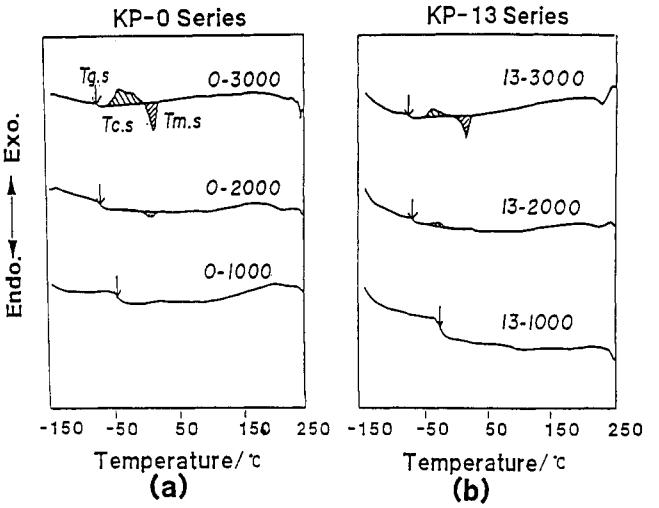

Figure 2. DSC thermograms of the (a) KP-0 and (b) KP-13 series. The arrows indicate the soft-segment glass transition temperatures, $T_{g,S}$. $T_{c,S}$ denote the crystallization and melting temperatures of the soft segment, respectively.

−150 to +250 °C. The heating rate was 5 °C/min. During the experiment, the sample was purged by nitrogen gas.

X-ray Diffraction/Scattering Measurements. Wide-angle X-ray diffraction (WAXD) patterns were taken with a Shimadzu GX3, operated at the power of 40 kV and 20 mA. Samples of 600 μm thick prepared by stacking thin films were exposed by Cu Kα radiation for 4 h, and the diffracted X-ray was recorded on a flat photographic film.

Small-angle X-ray scattering (SAXS) experiments were conducted with a 12-kW rotating-anode X-ray generator coupled with a one-dimensional position-sensitive detector. The sample to detector distance was 1.17 m, and the X-ray was monochromatized with a graphite crystal. The details of the apparatus were described elsewhere.[26] The observed SAXS data were corrected for air scattering, absorption, and thickness and then desmeared for a line-collimated incident X-ray beam. The absolute scattering intensity was then obtained by the nickel foil method.[27]

Infrared Spectroscopy. Transmission infrared spectrograms were obtained with a FIRIS 100 Fourier transform infrared spectrometer, Fuji Electric Co., Ltd. For measurements of stretched films, a stretching device designed in our laboratory was used, which is placed in a temperature-controlled heater block. The sample dimension was 10 mm long and 30 mm wide. The resolution and the number of scans were fixed to be 4 cm^{-1} and 64, respectively.

An attenuated total reflection spectroscopy (ATR) was also conducted with the same spectrometer by mounting an ATR attachment. A ZnSe crystal at the incident angle of 45° was mounted on the attachment as an internal reflection element (IRE). The resolution and the number of scans were 4 cm^{-1} and 512, respectively. The penetration depth is estimated to be ca. 1 μm.

III. Results and Discussion

III.1. Thermal Properties. Parts a and b of Figure 2 show DSC thermograms of the KP-0 and KP-13 series in a heating process, respectively, after cooling the sample from room temperature to −150 °C at a rate of ca. 10 °C/min. The soft-segment glass transition temperature, $T_{g,s}$, is indicated with an arrow. $T_{c,S}$ and $T_{m,S}$ denote the crystallization and melting temperatures of the soft segment, respectively. These characteristic temperatures of the KP-0 and KP-13 series obtained by DSC are listed in Table II. The hard-segment glass transition temperature was not detected. The hard-segment melting temperature appeared around 250 °C, where decomposition of the sample also took place. These temperatures are not tabulated in Table II. By increasing M_{PTMG}, $T_{g,S}$ decreases.

Table II
Characteristic Temperatures of the KP Series Obtained by DSC

code	$T_{g,S}$, °C	$T_{c,S}$, °C	$T_{m,S}$, °C
KP-0-1000	-47.7		
KP-0-2000	-67.7	-39.8	4.6
KP-0-3000	-82.7	-43.7	8.9
KP-13-1000	-52.0		
KP-13-2000	-72.2	-37.5	
KP-13-3000	-84.7	-45.8	11.6

This is a strong indication of the development of the degree of completion in microphase separation with increasing M_{PTMG}. The values of $T_{g,S}$ for the KP-13 series are slightly lower than those for the KP-0 series. This might suggest a higher degree of completion in microphase separation in the KP-13 series than in the KP-0 series. It is also worthy to note the appearance of crystallization exotherms in KP-0-3000 and KP-13-3000. This is explained as follows: In the process of a DSC experiment, the sample was cooled rapidly (ca. -10 °C/min) to -150 °C from ambient temperature. Therefore, some amounts of soft segments were quenched without crystallization. These crystallize during a DSC run at $T_{c,S}$, followed by melting at $T_{m,S}$. This speculation will be verified in the next section.

III.2. Mechanical Properties. Figure 3 shows stress–strain curves for the (a) KP-0 and (b) KP-13 series. As can be seen, both series behave similarly to each other, indicating that there is no remarkable effect of PES components. All curves show a typical stress–strain behavior as elastomers. The hard segments play as physical cross-link points, particularly in the case of those having high M_{PTMG}, i.e., KP-0-2000, KP-0-3000, KP-13-2000, and KP-13-3000. For KP-0-1000 and KP-13-1000, on the other hand, the strength at break is lower than the others. This indicates a low degree of completion in microphase separation compared to the others. The upturn behavior of KP-0-2000, KP-0-3000, KP-13-2000, and KP-13-3000 at around 400% elongation results from strain-induced crystallization of PTMG as will be discussed later. The similarity between KP-x-2000 and KP-x-3000 means that mechanically effective entanglements were attained for KP's having M_{PTMG} equal to or more than 2000.

By considering the fact that these materials are used at relatively low elongations (less than 100%) for medical use, the introduction of the PES component does not reduce the mechanical properties of this kind of polyurethane.

Figure 4 shows the temperature dependence of the storage moduli E' of the KP-0 (a) and KP-13 series (b). Each of the individual curves is roughly divided into three regions: glassy (1), glass transition (2), and rubbery plateau regions (3). Both series show no significant difference due to the presence of the PES component. For samples having a low M_{PTMG}, the modulus of the rubbery plateau region is lower than the others. One of the interesting aspects in these curves is the presence of a peak in the region 2 for KP-0-3000 and KP-13-3000. This fact was detected in the previous work[22] for KP-0-3000 and was explained by soft-segment crystallization. Here we look at this phenomenon in more detail by investigating the viscoelastic properties of KP's having different thermal histories.

Figure 5 shows the cooling rate dependence of temperature variations of the storage modulus, E', and loss tangent, tan δ, on heating for KP-0-3000, which has the largest crystallization exotherm, as shown in Figure 2a. Three samples of KP-0-3000 were prepared by cooling

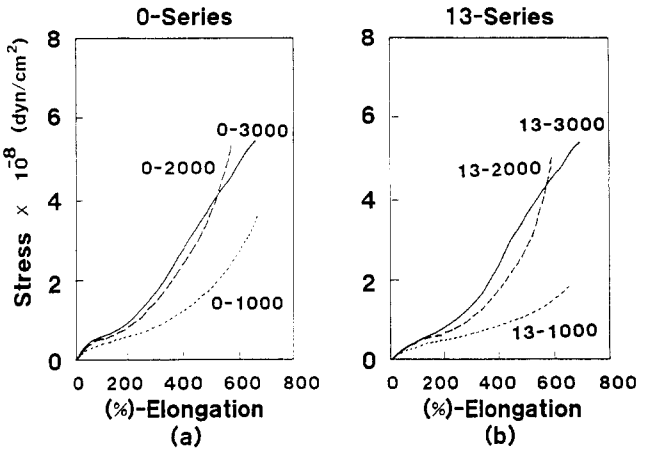

Figure 3. Stress–strain curves for the (a) KP-0 and (b) KP-13 series.

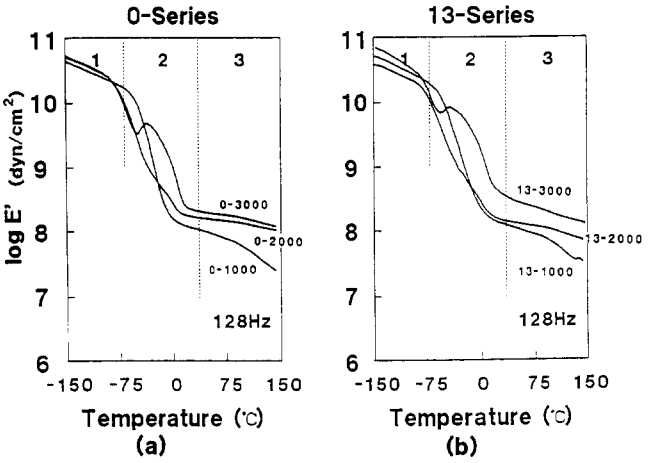

Figure 4. Temperature dependence of storage moduli E' for the (a) KP-0 and (b) KP-13 series.

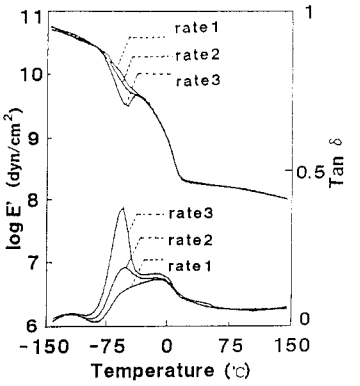

Figure 5. Cooling rate dependence of DSC thermograms on heating for KP-0-3000: rate 1, 1.7 °C/min; rate 2, 3.3 °C/min; rate 3, 10 °C/min.

from room temperature with different cooling rates: rate 1, 1.7 °C/min; rate 2, 3.3 °C/min; and rate 3, 10 °C/min. Rate 3 is the quickest quench of the three, and this rate is the same as the cases shown in parts a and b of Figure 4. By lowering the cooling rate, the peak in E' tends to be smeared out. The mechanical loss tangent, tan δ, in the samples having different cooling rates, also indicates a remarkable decrease in its peak around -60 °C. One can expect that the greater the cooling rate, the lower the degree of crystallization of the sample. Therefore, it is reasonable to deduce that the sample cooled with rate 3 could not have enough time to crystallize on cooling but crystallizes on heating during successive DSC or mechanical measurement.

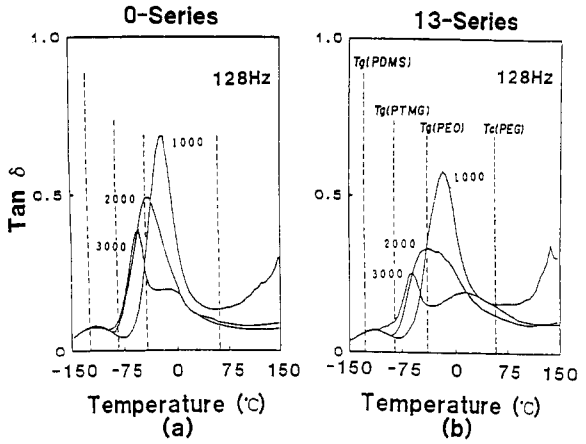

Figure 6. Temperature variation of loss tangent, tan δ, for the (a) KP-0 and (b) KP-13 series. The dashed lines indicate the literature values of the glass transition temperature, T_g, of the components.

Here we discuss the general feature of the viscoelastic properties of these samples. Figure 6 shows the temperature variation of tan δ for the (a) KP-0 and (b) KP-13 series. Contrary to Figure 4, one can find several differences between the KP-0 and KP-13 series in the behaviors of tan δ. Tan δ depends significantly on M_{PTMG} as well as the structure. The dashed lines drawn vertically in the figure indicate the literature values of the glass transition temperatures of the components,[28] i.e., PDMS, PTMG, and PEO, and the observed melting temperature of PEG.[29] The distinct maxima seen in each curve between −75 and 0 °C correspond to the glass transition of PTMG, which shifts to a lower temperature by increasing M_{PTMG} and approaches the literature value, −84 °C. This indicates that a microphase separation undergoes more in the samples having a higher M_{PTMG}. The second highest peaks seen in KP-0-3000 and KP-13-3000 at around 0 °C are related to melting of PTMG as discussed above. In the case of the KP-13 series, the peaks corresponding to the glass transition of soft segments are broadened by the presence of additional components such as PEO. The small peak around −130 °C is the amorphous relaxation due to local motions of methylene groups[30] and is not related to the glass transition of PDMS since this peak is observed for both the KP-0 and KP-13 series.

Figure 7 shows the master curves for the mechanical dispersion, tan δ, for the (a) KP-0 and (b) KP-13 series. The curves were constructed by shifting individual frequency dispersion curves obtained at several temperatures with respect to that at the reference temperature of −50 °C based on the assumption of the time–temperature superposition. ω and a_T are the frequency used in the dynamic mechanical measurement and the shift factor for the superposition, respectively. The highest peak seen in each figure corresponds to the glass transition of the soft segments (so-called β dispersion). The peak shifts toward the high-frequency and low-temperature side (from left to right) with increasing M_{PTMG}. It should be noted here that the width of the peak is broader for the KP-13 series than for the KP-0 series if the comparison is made at a given M_{PTMG}. This is due to the complex dispersion mechanisms for the KP-13 series arising from the presence of PEO components as discussed above. The dispersion located at around log ωa_T = 10–15 is assigned to the local motions of the methylene groups (γ dispersion). In the case of KP-0-3000 and KP-13-3000, an additional dispersion due to melting of PTMG is also clearly observed at around log ωa_T = −10 to −5.

The activation energy was estimated from the shift factor a_T. Table III shows the activation energies for β (glass transition of the soft segment) and γ (local motions of methylene groups) dispersions. The values are slightly different from those reported previously.[22] This is mainly due to some arbitrariness of the superposition and difference in the reference temperatures. In the previous work the reference temperature was taken as −5 °C, and here we used −50 °C, which is close to the glass transition temperature of the soft segment. The activation energies of β dispersion for the KP-13 series are larger than those for the KP-0 series by ca. 10 kcal/mol. The results of the viscoelastic and DSC measurements revealed that $T_{g,S}$ for the KP-13 series is lower than that for the KP-0 series. Therefore, the difference in the activation energy may result from a higher degree of completion in microphase separation for the KP-13 series than for the KP-0 series in addition to the presence of PEO segments, which may also raise the activation energy.

Figure 8 shows the comparison of the M_{PTMG} dependence of $T_{g,S}$ observed by DSC and viscoelastic measurements. The systematic difference between the two techniques is due to the methods employed. In the case of viscoelasticity, $T_{g,S}$ is expected to approach that observed by DSC with lowering the frequency of the mechanical agitation from 128 Hz to an infinitesimally low frequency. $T_{g,S}$ decreases with increasing M_{PTMG} and approaches that for pure PTMG, as indicated with a dash-dotted line. The fact that $T_{g,S}$ for KP-13 is lower than that for KP-0 indicates that the degree of completion in microphase separation for the KP-13 series is higher than that for the KP-0 series. This corresponds to the fact shown in Table III; i.e., the activation energy for the glass transition of the soft segments is higher for the KP-13 series than for the KP-0 series.

III.3. X-ray Diffraction/Scattering. Figure 9 shows the wide-angle X-ray diffraction patterns for undrawn and drawn films of KP-0-2000 and KP-13-2000. ED indicates the elongation direction. The diffraction intensity is stronger in KP-0-2000 than in KP-13-2000. This is due to the stronger absorption due to the sample owing to the PDMS component in the latter. Debye–Scherrer rings due to the amorphous halo of the soft segments[31] are seen in the photographs for undrawn films, which disappear by drawing. In the pattern for 400% drawn films, two sets of diffraction maxima located on the equator are clearly observed. The appearance of these diffraction maxima indicates that strain-induced crystallization takes place by elongation, as was suggested in the stress–strain curves (Figure 3). The outer and inner spots give the spacing of 3.6 and 4.3 Å, respectively. These spots are assigned to be the (010) and (100) diffractions of PTMG.[32] No diffraction maximum due to the hard segments was detected. This may be due to a low content and a low degree of completion in the crystallization of the hard segments as reported by Ishihara et al.[12]

Figure 10 shows SAXS profiles for the (a) KP-0 and (b) KP-13 series. Since the samples had no preferential orientation, the ordinate was taken to be the so-called Lorentz-corrected scattered intensity, $s^2I(s)$. $I(s)$ and s mean the absolute scattered intensity and the magnitude of the scattering vector, which is given by $s = (2 \sin \theta)/\lambda$, respectively. θ and λ are half the scattering angle and the wavelength of X-ray, respectively. Each curve has a scattering maximum, indicating the presence of the microphase-separated structure. In the case of samples having low PTMG molecular weights, i.e., KP-0-1000 and KP-13-1000, the peak height is relatively low. Therefore, the correlation hole effect,[23,24,33] which also gives rise to

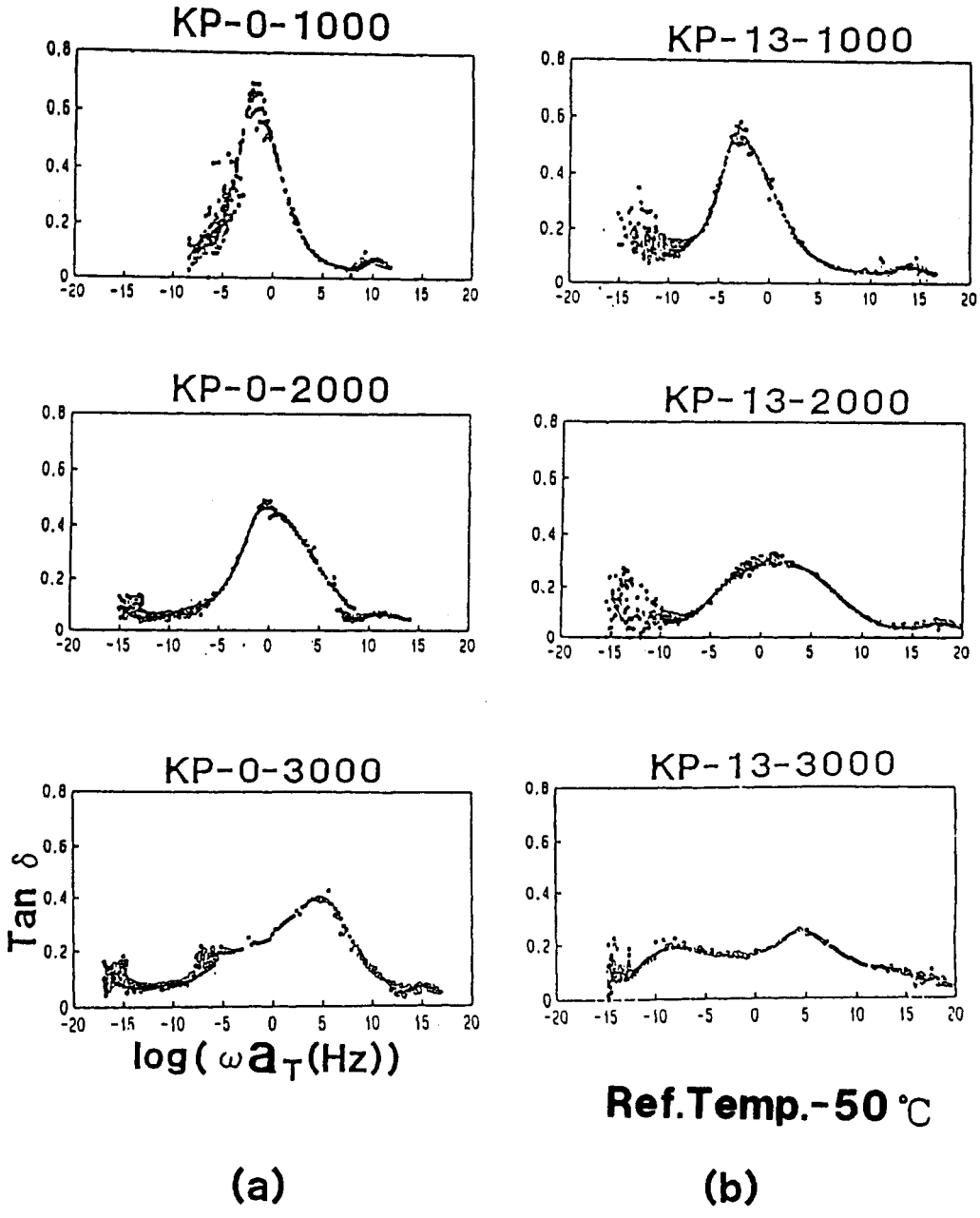

Figure 7. Master curves for the mechanical dispersion, tan δ, for the (a) KP-0 and (b) KP-13 series.

Table III
Apparent Activation Energies of Mechanical Dispersion

code	dispersion, kcal/mol	
	main	local
KP-0-1000	39.1	7.3
KP-0-2000	33.4	8.2
KP-0-3000	37.0	8.8
KP-13-1000	46.6	7.1
KP-13-2000	45.6	7.6
KP-13-3000	54.5	5.2

a scattering maximum even with the absence of the microphase-separated structure, may have to be taken into account. In general, however, one can conclude that the microphase-separated structure is more developed in samples having a higher M_{PTMG}. The long spacing, d, was estimated from the peak maximum, which was in the range from 100 to 150 Å. Further discussion on the sizes of the microphase-separated structure will be done in a later section.

III.4. Infrared Absorption Spectroscopy. Since infrared absorption spectra for segmented poly(urethanes)

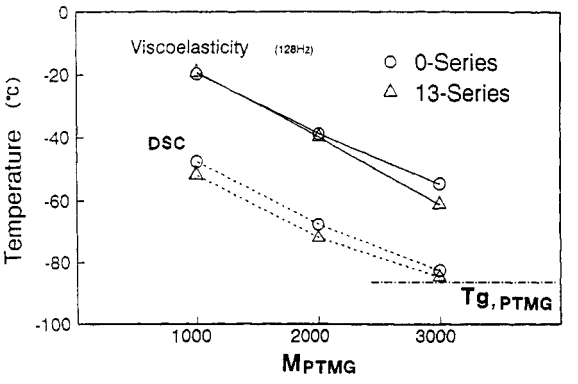

Figure 8. Comparison of PTMG molecular weight dependence of $T_{g,S}$ observed by DSC (solid line) and viscoelastic (dashed line) measurements, respectively. The dash-dot-dashed line indicates the glass transition temperature of pure PTMG.

are well assigned, one can easily estimate the apparent fraction of the hydrogen bonding.[10,18,34] Here we estimate the index of hydrogen bonding, H_{UT}, by taking the ratio of the absorbances of the hydrogen-bonded urethane car-

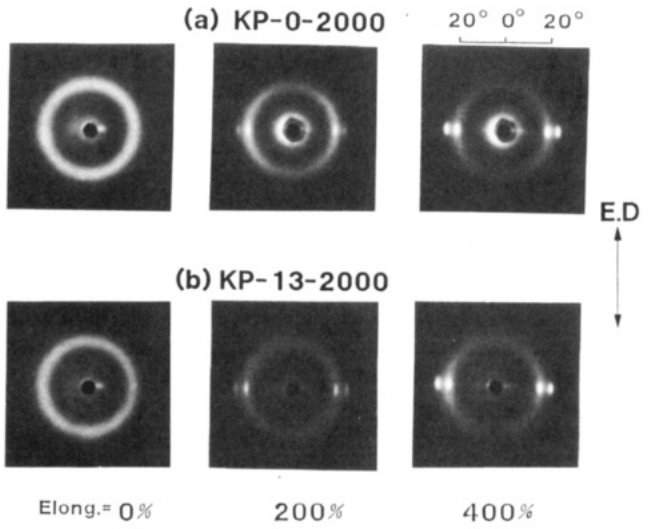

Figure 9. Wide-angle X-ray diffraction patterns for undrawn and drawn films of (a) KP-0-2000 and (b) KP-13-2000. ED indicates the stretching direction.

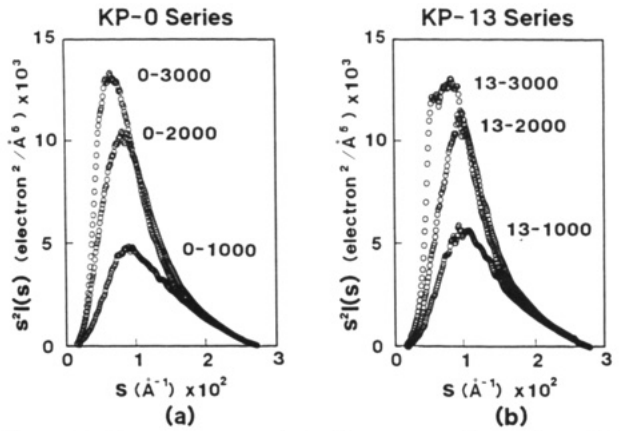

Figure 10. Lorentz-corrected absolute scattered intensity, $s^2I(s)$, vs the magnitude of the scattering vector, s, plots for the (a) KP-0 and (b) KP-13 series.

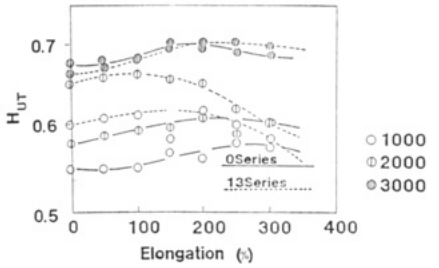

Figure 11. Elongation dependence of H_{UT} for the KP-0 and KP-13 series. The solid and broken lines correspond to KP-0 and KP-13, respectively.

bonyl groups with respect to the total absorbances for urethane groups, i.e.

$$H_{UT} = \frac{A[\nu(C{=}O)^b]}{A[\nu(C{=}O)^b] + A[\nu(C{=}O)^f]} \quad (1)$$

where $A[\nu(C{=}O)^b]$ and $A[\nu(C{=}O)^f]$ are the absorbances due to the stretching vibrations of the hydrogen-bonded and hydrogen-bond-free urethane carbonyl groups, respectively. Figure 11 shows the elongation dependence of H_{UT} for the KP-0 and KP-13 series. The solid and broken lines correspond to KP-0 and KP-13, respectively. Although H_{UT} is more or less invariant against elongation except for KP-13-1000 and KP-13-2000, it depends clearly on M_{PTMG}. The higher the M_{PTMG}, the higher the H_{UT}.

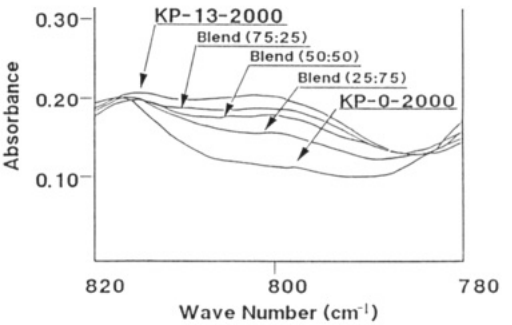

Figure 12. Attenuated total reflection (ATR) spectrograms for blends of KP-13-2000 and KP-0-2000.

This indicates that hard-segment domains in a sample having a higher M_{PTMG} are developed better than that having a low M_{PTMG}, which is again in good agreement with the results of DSC, viscoelastic, and SAXS measurements. By comparison of the KP-0 and KP-13 series, H_{UT} is more likely higher for the latter than for the former, which also indicates that the degree of completion in microphase separation is higher for the KP-13 than the KP-0 series. However, H_{UT} for KP-13-1000 and for KP-13-2000 decreases steeply by stretching, which has not been well understood at this stage.

ATR measurements for blends of KP-0-2000 and KP-13-2000 were also conducted with an IRE made of a ZnSe crystal having a refractive index $n = 2.4$. The penetration depth is estimated to be ca. 1 μm. An IRE made of a Ge crystal ($n = 4.0$) would be better for characterizing a thinner surface. However, a Ge crystal cannot be used for this wavenumber region since it has an absorption of around 800 cm^{-1}. Figure 12 shows FTIR-ATR spectrograms for blends of KP-13-2000 and KP-0-2000. The range of the wavenumber region was chosen to be 780–820 cm^{-1} so as to visualize the absorption bands for the Si–O stretching vibration at around 805 cm^{-1}. The blend ratio is indicated in the figure. Blend x:y means a blend film composed of x and y percentages of KP-13-2000 and KP-0-2000 by weight. In the case of KP-13-2000, a broad maximum is detected at around 805 cm^{-1}, corresponding to the Si–O stretching vibration. This peak decreases gradually by increasing the KP-0-2000 component. By assuming additivity between spectrograms in this wavenumber region (780–820 cm^{-1}), we estimated the surface concentration of KP-13 with a curve-fitting method as described elsewhere.[35] Figure 13 shows the surface composition of KP-13-2000 as a function of its bulk composition. The diagonal line indicates the case where no selectivity occurs at the surface. This kind of surface selectivity was observed both on the free surface and on the substrate-faced surface (in this particular case, a glass plate). The enrichment of the KP-13 series on both surfaces is attributed to a low surface free energy of the PDMS component in the KP-13 series. Surface enrichment of polyurethane containing a PDMS component for films prepared by casting a solution was studied by Matsuda et al.[36] by X-ray photoelectron spectroscopy (XPS). The depth of the enrichment detected by XPS is less than 100 Å. Since the penetration depth, d_p, in our ATR measurements is estimated to be ca. 1 μm when a ZnSe crystal cut by 45° is used, this surface-enrichment effect goes over the depth of this order. This indicates that a strong interaction between polymer chains and the substrate or air surface is present in solution and remains during the solidification process of the polymer without decreasing the interaction distance on the order of microns. This is surprisingly inconsistent with the physical intuition that the correlation length, in other

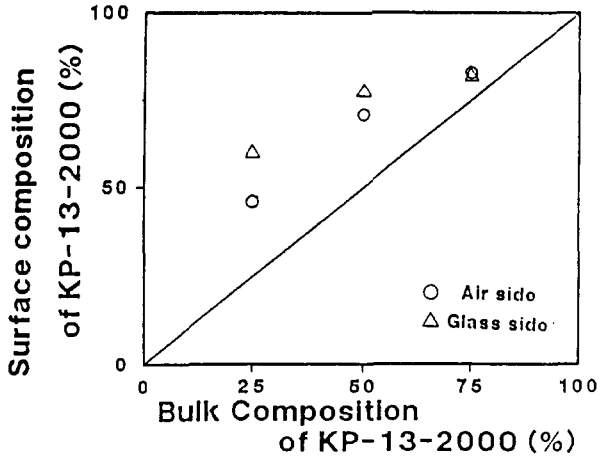

Figure 13. Surface composition of KP-13-2000 as a function of its bulk composition. The diagonal line indicates the case where no selectivity occurs at the surface.

words, the persistent distance of the polymer–polymer interaction, decreases with polymer concentration. A similar phenomenon, i.e., surface enrichment of one component in blends over a micron order, however, was found in blends of cellulose and poly(vinyl alcohol).[35]

IV. Estimation of Sizes of Soft- and Hard-Segment Domains

The characterization of the microphase-separated structure of polyurethane and/or poly(urethaneurea) is very important to the understanding of those mechanical properties. Sizes of soft and hard segments have been evaluated by using either electron microscopy[20,37] or small-angle scattering techniques, such as SAXS[7,11,12] and/or small-angle neutron scattering.[13] In most cases, microdomain structures of polyurethane and poly(urethaneurea) are modeled with rodlike or lamellalike domains of hard segments embedded in a soft-segment matrix. The long spacing is reported to be around 100–150 Å, and the hard-segment length is estimated to be ca. 100 Å.[7,11,12]

In the case of block or graft copolymers, including multiblock copolymers, the domain size is well predictable by means of the degree of polymerization, Z, the segment length, b, and the Flory interaction parameter, χ. Here we try to estimate the sizes of the soft- and hard-segment domains semiquantitatively. According to Hashimoto et al.,[38,39] the domain size is given by

$$d_K \simeq b_K Z_K^{2/3} \tag{2}$$

in the strong segregation limit. Z_K and b_K are the number-average degree of polymerization and the segment length of component K where K is H (hard segment) and S (soft segment), respectively. The long spacing of the microdomains, d, can be roughly estimated to be

$$d \simeq d_S + d_H \tag{3}$$

Let us estimate d_S and d_H by assuming two extreme cases; (A) d_H is proportional to M_{PTMG} and (B) d_H is constant irrespective of M_{PTMG}. Since the weight fraction of the total amount of MDI + EG was kept constant and the sequence of the MDI–EG unit is rather rigid, case A is more probable. In case A, the following equation is given:

$$d \simeq b_S Z_{n,S}^{2/3} + b_H Z_H \tag{4}$$

The requirement of the constant weight fraction of MDI + EG leads to

$$Z_H = aZ_S \tag{5}$$

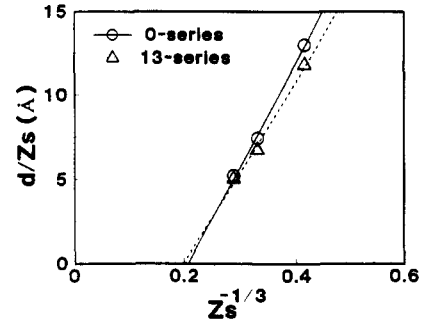

Figure 14. Variation of d/Z_S as a function of $Z_S^{-1/3}$.

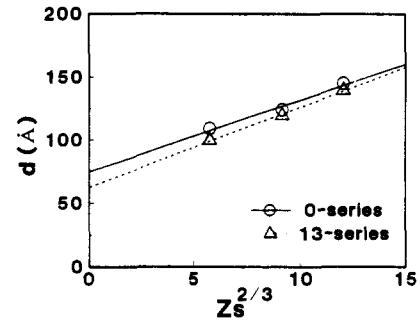

Figure 15. Variation of d as a function of $Z_S^{2/3}$.

where a is a constant and is given by

$$a = (1/f - 1)(m_S/m_H) \tag{6}$$

f, m_S, and m_H are the weight fraction of MDI–EG and molecular weights of the tetramethylene glycol and MDI–EG segments, respectively. Therefore

$$d \simeq b_S Z_S^{2/3} + b_H a Z_S \tag{7}$$

By dividing both sides with Z_S, one gets

$$d/Z_S \simeq b_S Z_S^{-1/3} + b_H a \tag{8}$$

Figure 14 shows the variation of d/Z_S with $Z_S^{-1/3}$. Although the data points fall on a straight line for both series, the values of the intercept are −12.7 and −10.7 Å, respectively, for the KP-0 and KP-13 series. Since the intercept should be positive ($b_H > 0$ and $a > 0$), this fact strongly suggests the unreality of assumption A. Hence, the hard-segment domain size does not seem to be influenced linearly by M_{PTMG}.

On the other hand, if d_H is more or less constant irrespective of M_{PTMG} (case B), one gets the relation between the long spacing d and the individual domain size as follows:

$$d \simeq b_S Z_S^{2/3} + d_H \tag{9}$$

Kimura et al.[7] assumed the invariance of d_H and estimated d_H and d_S. However, eq 10 is different from that used by Kimura et al. In their case, the samples were highly stretched and heat treated before relaxing. Therefore, they assumed that d_S varied with Z_S instead of $Z_S^{2/3}$. This relation is not applicable to our case because the PTMG chains are flexible polymer chains in a confined space (microdomains) as discussed above. Figure 15 shows the variation of d as a function of the $^2/_3$ power of the degree of polymerization of the soft segment, $Z_S^{2/3}$. As can be seen in the figure, the estimated values by SAXS fall onto a straight line in the cases for both the KP-0 and KP-13 series, respectively. The strong Z_S dependence of d indicates that the soft-segment domain (or matrix) is composed of PTMG (for the KP-0 series) or a mixture of

Table IV
Estimated Domain Sizes, d_S and d_H, and the PTMG Segment Length, b_{PTMG}

	M_{PTMG}	Z_S	d_S, Å	d_H, Å	b_{PTMG}, Å
KP-0-1000	1025	14.2	34.3		
KP-0-2000	2000	27.8	49.3	74.9	5.69
KP-0-3000	2950	41.0	70.1		
KP-13-1000	1025	14.2	37.3		
KP-13-2000	2000	27.8	56.8	62.8	6.33
KP-13-3000	2950	41.0	77.0		

PTMG and PES (for the KP-13 series) without any chain extension with MDI–EG–MDI. In addition, d_S is ruled by M_{PTMG} even in the case of the KP-13 series, where the molecular weight of PES is constant. This may result from the low PES fraction in the system.

Considerable amounts of PTMG and PES chains having MDI at both ends should be linked to each other with EG and bridge two separate hard-segment domains. However, most of PTMG (or PES) chains start from a boundary of a hard-segment domain and end at the same or a different boundary. Since this arrangement of the hard-segment domains is regular enough to give rise to coherency in SAXS, the interdomain distance is selectively detected by SAXS. Otherwise, d should not depend systematically on Z_S. The slope and intercept of this plot give the segment length of the soft segment, b_S, and the hard-segment domain size, d_H, respectively. The estimated b_S and d_H are listed in Table IV. Although the value of Z_S studied here might to be too small to apply the scaling rule (eq 9), the estimated segment lengths are 5.69 and 6.33 Å, respectively, for the KP-0 and KP-13 series and are close to the literature value for PTMG, b_{PTMG} = 7.30 Å.[28] This result supports the validity of assumption B. The hard-segment domain size was estimated to be 74.9 and 62.8 Å, respectively, for KP-0 and KP-13. Since the contour length of MDI–EG is estimated to be roughly 17 Å,[12] the hard segment may consist of ca. four successive units of MDI–EG on average. The reason why d_H for the KP-0 series is different from that for the KP-13 series is not clear at this stage.

In case B, d_H has to be constant irrespective of the contradictory requirement, i.e., the constant chemical composition irrespective of M_{PTMG}. This problem is solved by folding the hard segments as depicted by Koberstein et al. (Figure 23 of ref 11). The lateral dimension of the hard-segment domain changes with M_{PTMG}. The higher the M_{PTMG}, the larger the lateral dimension of the hard-segment domains so as to keep the volume (or weight) fraction of the hard-segment domains constant. The increase in the lateral dimension with M_{PTMG} should reflect the degree of phase separation and the index of the hydrogen bond, which are clearly elucidated in DSC (Figure 2), viscoelastic properties (Figures 6 and 7), SAXS profiles (Figure 10), and FTIR analyses (Figure 11).

V. Conclusions

The degrees of completion in microphase separation for segmented polyurethanes having PES components in the main chain were investigated by mechanical and thermal analyses, Fourier transform infrared absorption spectroscopy (FTIR), and small-angle X-ray scattering (SAXS) techniques. These results were compared with those for PES-free polyurethanes having the same molecular weight of the soft segment, M_{PTMG}.

Systematic variations in the mechanical and thermal properties were found with M_{PTMG}. The higher the M_{PTMG}, the lower the soft-segment glass transition, i.e., the higher the degree of completion in microphase separation. The KP-13 series, i.e., polyurethanes containing a PES component, has a complicated chemical structure. The PES component in the soft segment reduces the capability of crystallization of PTMG but raises the degree of completion in microphase separation between the soft and hard segments. This is proven by the higher activation energy for glass transition of the soft segment in the KP-13 than KP-0 series and by the higher hydrogen-bonding index, H_{UT}. On the basis of these results, we conclude that PES block chains are dispersed in the matrix of the major soft segment, PTMG, and play as an enhancement reagent of microphase separation between soft and hard segments.

The SAXS analyses indicate that the size of the soft-segment domain (or matrix) obeys the $^2/_3$-power rule, which applies to microphase-separated block copolymers in the strong segregation limit. The hard-segment domain size was estimated to be ca. 70 Å irrespective of M_{PTMG}, which corresponds to ca. four units of MDI–EG. The hard segment may be folded back and forth in the hard-segment domain so as to keep the constant thickness of the hard-segment domain.

By blending the KP-13-2000 and KP-0-2000 series, surface enrichment of KP-13-2000 was detected by FTIR-ATR. The range of surface enrichment is on the order of 1 μm, which is much larger than the individual polymer chains. This suggests that the surface enrichment is originated from a strong interaction between the polymer and either substratum or air during the solidification process of the sample film. This kind of surface enrichment might be applied to a surface property modification of polymer film by blending.

Acknowledgment. We are grateful to Prof. T. Hashimoto, Department of Polymer Chemistry, Kyoto University, for his kind arrangement of the SAXS apparatus and to Dr. Hiramatsu, Central Research, Kanegafuchi Chemical Industry Co., Ltd., Kobe, Japan, for supplying the samples. We acknowledge the financial support of the Ministry of Education, Science, and Culture of Japan, under Grant 01460229, and of Resources and Environment Protection Research Laboratory, NEC Corp., Kawasaki, Japan.

References and Notes

(1) For example: Ratner, B. D. In *Comprehensive Polymer Science*; Aggarwal, S. L., Ed.; Pergamon: New York, 1989; Vol. 7, Chapter 7.
(2) Planck, H.; Egbers, G.; Syre, I. *Polyurethanes in Biomedical Engineering*; Elsevier: Amsterdam, The Netherlands, 1984.
(3) Lelah, M. D.; Cooper, S. L. *Polyurethanes in Medicine*; CRC Press: Boca Raton, FL, 1986.
(4) Clogh, S. B.; Schneider, N. S. *J. Macromol. Sci., Phys.* **1968**, *B2*, 553.
(5) Huh, D. S.; Cooper, S. L. *Polym. Eng. Sci.* **1971**, *11*, 36.
(6) Cooper, S. L.; Seymour, R. W. In *Block and Graft Copolymers*; Burke, J. J., Weiss, V., Eds.; Syracuse University Press: Syracuse, NY, 1973.
(7) Kimura, I.; Ishihara, H.; Ono, H.; Yoshihara, N.; Nomura, S.; Kawai, H. *Macromolecules* **1974**, *7*, 355.
(8) Sung, C. P. S.; Smith, T. W.; Sung, N. H. *Macromolecules* **1980**, *13*, 117.
(9) Hoffman, K.; Bonart, R. *Makromol Chem.* **1983**, *184*, 1529.
(10) Wang, C. B.; Cooper, S. L. *Macromolecules* **1983**, *16*, 775.
(11) Koberstein, J. T.; Stein, R. S. *J. Polym. Sci., Polym. Phys. Ed.* **1983**, *21*, 1439.
(12) Ishihara, H.; Kimura, I.; Yoshihara, N. *J. Macromol. Sci., Phys.* **1983–1984**, *B22*, 713.
(13) Miller, J. A.; Cooper, S. L.; Han, C. C.; Pruckmayr, G. *Macromolecules* **1984**, *17*, 1063.
(14) Miller, J. A.; Lin, S. B.; Hwang, K. K. S.; Wu, K. S.; Gibson, P. E.; Cooper, S. L. *Macromolecules* **1985**, *18*, 32.

(15) Desper, C. R.; Schneider, N. S.; Jasinski, J. P.; Lin, J. S. *Macromolecules* **1985**, *18*, 2755.
(16) Miller, J. A.; Cooper, S. L. *J. Polym. Sci., Polym. Phys. Ed.* **1985**, *23*, 1065.
(17) Takahara, A.; Tashita, J.; Kajiyama, T.; Takayanagi, M.; MacKnight, W. J. *Polymer* **1985**, *26*, 987.
(18) Shibayama, M.; Kawauchi, T.; Kotani, T.; Nomura, S.; Matsuda, T. *Polym. J.* **1986**, *18*, 719.
(19) Shibayama, M.; Ohki, Y.; Kotani, T.; Nomura, S. *Polym. J.* **1987**, *19*, 1067.
(20) Li, C.; Cooper, S. L. *Polymer* **1990**, *31*, 3.
(21) Kira, K.; Minokami, T.; Yamamoto, N.; Hayashi, K.; Yamashita, I. *Seitaizairyo (Biomaterials)* **1983**, *1*, 29.
(22) Shibayama, M.; Inoue, M.; Yamamoto, T.; Nomura, S. *Polymer* **1990**, *31*, 749.
(23) Leibler, L. *Macromolecules* **1980**, *13*, 1602.
(24) Mori, K.; Tanaka, H.; Hashimoto, T. *Macromolecules* **1987**, *20*, 381.
(25) Hiramatsu, K.; Kira, K. Private communication.
(26) Hashimoto, T.; Suehiro, S.; Shibayama, M.; Saijo, K.; Kawai, H. *Polym. J.* **1981**, *13*, 501.
(27) Hendricks, R. W. *J. Appl. Crystallogr.* **1972**, *5*, 315.
(28) Brandrup, J.; Immergut, E. H. *Polymer Handbook*, 3rd ed.; Wiley: New York, 1989.
(29) Unpublished results.
(30) McKenna, L. W.; Kajiyama, T.; MacKnight, W. J. *Macromolecules* **1969**, *2*, 58. Kajiyama, T.; MacKnight, W. J. *Macromolecules* **1969**, *2*, 254.
(31) Bonart, R. *J. Macromol. Sci., Phys.* **1968**, *B2*, 115.
(32) Imada, I.; Miyakawa, T.; Chatani, Y.; Tadokoro, H.; Murahashi, S. *Makromol. Chem.* **1965**, *83*, 113.
(33) de Gennes, P.-G. *Scaling Concepts in Polymer Physics*; Cornell University Press: Ithaca, NY, 1979.
(34) Yamamoto, T.; Shibayama, M.; Nomura, S. *Polym. J.* **1989**, *21*, 895.
(35) Shibayama, M.; Yamamoto, T.; Xiao, C.; Sakurai, S.; Hayami, A.; Nomura, S. *Polymer* **1991**, *32*, 1010.
(36) Matsuda, T. Private communication.
(37) Chen-Tsai, C. H. Y.; Thomas, E. L.; MacKnight, W. J.; Schneider, N. S. *Polymer* **1986**, *27*, 659.
(38) Hashimoto, T.; Shibayama, M.; Kawai, H. *Macromolecules* **1980**, *13*, 1237.
(39) Hashimoto, T.; Shibayama, M.; Kawai, H. *Macromolecules* **1983**, *16*, 1093.

Registry No. KP-13, 121939-43-3; KP-0, 135929-14-5.